

Phase diagram of vortex matter of type-II superconductors

X. B. Xu,^{1,*} H. Fangohr,² S. Y. Ding,¹ F. Zhou,¹ X. N. Xu,¹ Z. H. Wang,¹ M. Gu,¹ D. Q. Shi,³ and S. X. Dou³

¹*Department of Physics, National Laboratory of Solid State Microstructures, Nanjing University, Nanjing 210093, People's Republic of China*

²*School of Engineering Sciences, University of Southampton, Southampton SO17 1BJ, United Kingdom*

³*Institute for Superconducting and Electronic Materials, University of Wollongong, NSW 2522, Australia*

(Received 28 September 2010; published 3 January 2011)

We propose a model to construct the phase diagram for type-II superconductors through molecular-dynamics simulation. In this model, the Abrikosov vortices interact with long-range repulsion and short-range attraction. We are able to obtain the phase diagrams consisting of the vortex lattice, the intermediate-mixed phase (IMP), and the disordered vortex phase in the B - T , B - κ , and B - q planes, where B is induction, κ is the Ginzburg-Landau parameter, and q is the relative strength of the attraction to repulsion interactions between vortices. The IMP is in the form of a superlattice of either vortex bubbles or parallel vortex stripes, agreeing excellently with experimental results that have not yet been explained by existing models.

DOI: [10.1103/PhysRevB.83.014501](https://doi.org/10.1103/PhysRevB.83.014501)

PACS number(s): 74.25.Dw, 74.25.Uv

Type-II superconductors exhibit a set of interesting phases including the Shubnikov phase, which has attracted a large amount of experimental and theoretical attention.¹ In the phenomenological Ginzburg-Landau-Abrikosov-Gor'kov (GLAG) theory, it is proposed that the Shubnikov phase is the Abrikosov vortex lattice (the mixed phase) in superconductors with a high Ginzburg-Landau (GL) parameter, κ , which has been well confirmed by experiments.²⁻⁴ Further study shows that the Shubnikov phase can be either the mixed phase or the intermediate-mixed phase (IMP), consisting of a combination of the mixed phase and the Meissner phase for low- κ type-II superconductors. Therefore, type-II superconductors are divided into two kinds: type II/1, which exhibits the IMP, and type II/2, which exhibits the mixed phase.⁴ The Abrikosov vortex lattice is found in the limits of high temperatures ($T \approx T_c$, the critical temperature), high fields ($B \approx B_{c2}$, the upper critical field), and for a very short electron mean free path ($\kappa \gg 1$) based on the GLAG theory, which is widely used to study type-II/2 superconductors. Great efforts have been devoted to overcoming these restrictions. Substantial progress has indeed been made. For example, the calculation of the vortex lattice and its elastic properties at arbitrary fields and κ has been reported.⁴ However, one still expects a more generic theory.

With the discovery of new high- κ oxide superconductors, the vortex liquid phase was observed.^{5,6} An interesting feature of the vortex liquid is so-called reentrance, in which the vortex liquid phases occur at both high- and low-field regions at a constant temperature. This reentrant behavior has also been observed in the low- κ classical superconductor NbSe₂.^{7,8} Simulations have suggested that the reentrance phenomenon can result from the disorders in the anisotropic and layered high- κ type-II superconductors,⁹ but the nature of the reentrance of vortex melting is still a matter of controversy.

As a new vortex phase, the IMP was initially observed in low- κ type-II superconductors such as Nb, V, Tc, and Pb alloys with $\kappa \approx 1/\sqrt{2}$.¹⁰⁻¹³ Although the IMP has been associated with the existence of the short-range attractive interaction between vortices in addition to the long-range repulsive interaction,^{12,14} a comprehensive understanding of the physics of the IMP is still lacking. For example, to the best of our knowledge, no numerical phase diagram of the

type-II/1 superconductors, that is, the phase diagram for the IMP, has been reported. It should be noted that a rich variety of physical and chemical systems display the so-called modulated structures similar to the IMP, originating from a compromise of the competing interactions.¹⁵⁻¹⁷ For instance, the presence of a short-range attraction and of a screened electrostatic repulsion leads to the formation of aggregates (bubbles) in charged colloidal suspensions.¹⁸ For other areas, note the following: (i) The effective interaction (short-ranged attraction and long-ranged repulsion) between two solute particles in a subcritical liquid solvent can stabilize clusters of nanometer sizes.¹⁹ (ii) Spontaneous patterning of quantum dots at the air-water interface occurs due to the competition between an attraction and a longer-ranged repulsion.²⁰ Therefore, by studying the consequences of the presence of the competing interactions in a system of superconducting vortices, it may be possible to gain insight into the nature of vortex phases including the IMP.

An important prediction of the GLAG theory is that there exist two kinds of superconductors: a superconductor with $\kappa < 1/\sqrt{2}$ belongs to type I, and one with $\kappa > 1/\sqrt{2}$ belongs to type II. Now that the IMP was observed only for low- κ type-II superconductors ($\kappa \approx 1/\sqrt{2}$), a complete theory should be able to predict the IMP at low κ and the mixed phase at high κ . To the best of our knowledge, there is no such work published. Thus, it is still a long-standing challenge to understand the previously mentioned vortex phases in a unified frame, especially at the microscopic level.

Here, we study the equilibrium phase diagram of type-II (type-II/1 and type-II/2) superconductors by Langevin molecular-dynamical simulation. The molecules are two-dimensional Abrikosov vortices interacting with each other, showing long-range repulsion with short-range attraction. We study the vortex phases with a unified model as a function of vortex density, temperature, κ , and the relative strength of the attraction to repulsion, q . In the B - T plane, we find that the vortex system with competing interactions forms the vortex lattice at high fields, the IMP at intermediate fields, and the disordered vortex phase in high temperatures and low fields; in the B - κ and B - q planes, a disordered vortex phase occurs in lower fields, and the IMP and the vortex lattice occur in higher fields. This indicates that we have calculated all vortex

phases observed experimentally for type-II/1 and type-II/2 superconductors.

Our main assumption is that the effective interaction force between two vortices is as follows:^{21,22}

$$F^{vv}(\mathbf{r}) = (\phi_0^2 s)(2\pi\mu_0\lambda^3)^{-1}[\lambda/\mathbf{r} - q \exp(-\mathbf{r}/\xi)], \quad (1)$$

where ϕ_0 is the flux quantum, s is the length of the vortex, μ_0 is the vacuum permeability, λ is the London penetration depth, and ξ is the effective coherence length. The first term is a long-ranged repulsion via the logarithmic form potential,²³ the second term is the short-ranged vortex attraction of an exponential form,¹¹ and the parameter q reflects the relative strength of the attraction to repulsion interactions. Then we use the overdamped Langevin equation of motion for a vortex at position \mathbf{r}_i ,²⁴

$$\mathbf{F}_i = \sum_j^{N_v} \mathbf{F}^{vv}(\mathbf{r}_i - \mathbf{r}_j) + \sum_k^{N_p} \mathbf{F}^{vp}(\mathbf{r}_i - \mathbf{r}_k^p) + \mathbf{F}_i^T = \eta \frac{d\mathbf{r}_i}{dt},$$

where \mathbf{F}_i is the total force acting on vortex i , \mathbf{F}^{vp} are the forces due to vortex-pin interactions, \mathbf{F}^T is the thermal stochastic force, η is the Bardeen-Stephen friction coefficient, N_v is the number of vortices, N_p is the number of pinning centers, and \mathbf{r}_k^p is the position of the k th pinning center. We employ periodic boundary conditions and cut off the vortex-vortex interaction potential smoothly.²⁵ Pinning centers exert an attractive force on the vortices: $\mathbf{F}^{vp}(\mathbf{r}_i - \mathbf{r}_k^p) = -f_{pv}(r_{ik}/r_p) \exp[-(r_{ik}/r_p)^2] \hat{\mathbf{r}}_{ik}$, where f_{pv} tunes the strength of this force and r_p determines its range. We assume $r_p = 0.5\lambda$ and $f_{pv} \propto B_{c2}^2(1 - B/B_{c2})\xi^2/\kappa^2$ as core pinning is considered,²⁶ where $\kappa = \lambda/\xi$, and B_{c2} , λ , and ξ depend on the temperature via $B_{c2}(T) = B_{c2}(0)[1 - (T/T_c)^2]$, $\lambda(T)/\lambda(0) = (1 - T/T_c)^{-1/2}$, and $\xi(T)/\xi(0) = (1 - T/T_c)^{-1/2}$.²⁷ The thermal fluctuation force is implemented with a Box-Müller random number generator and has properties $\langle F_i^T \rangle = 0$ and $\langle F_i^T(t)F_j^T(t') \rangle = 2\eta k_B T \delta_{ij} \delta(t - t')$ at a given temperature T . We normalize lengths by $\lambda_0 = \lambda(0)$ and time by $\tau_0 = 2\pi\mu_0\eta_0\lambda_0^4/(\phi_0^2 s)$. The equation of motion is integrated by an Euler scheme with a normalized time step of $\Delta t = 0.005$.²⁸ The total number of vortices $N_v = 900$ (unless specified otherwise) is used in the calculations presented here. For larger systems, similar results are observed. We employ $q = 2.3$, $N_p = N_v$, $f_{pv} = 0.1f_0$ (unless specified otherwise), $\xi_0 = 200 \text{ \AA}$, $\lambda_0 = 200 \text{ \AA}$, $s = 12 \text{ \AA}$, and $\eta_0 = 1.4 \times 10^{-17} \text{ kg/s}$. In all cases, the vortices are randomly distributed for the initial state of the superconducting system. Pinning centers are randomly distributed in the simulation box. In addition, we calculated the vortex phases by replacing the logarithmic form vortex-vortex potential with the modified Bessel function of the second kind [$K_0(r/\lambda)$], and found that the simulating results for the modified Bessel function are in qualitative agreement with those for the logarithmic function. Thus, the simulation results in this work are applicable to two-dimensional systems (thin films, stack of superconducting layers) and quasi-two-dimensional systems (rigid vortex lines).

The equilibrium phase diagram of type-II superconductors in the B - T plane is shown in Fig. 1, and the details of the phases in regimes I, II, II, and IV in Fig. 1 can be seen in Fig. 2. The phase diagram demonstrates all the well-known vortex phases for type-II/1 and type-II/2 superconductors,

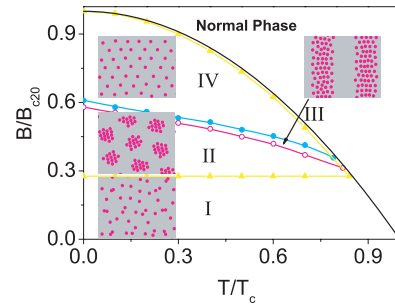


FIG. 1. (Color) Phase diagram of vortex matter as a function of field and temperature. The insets show the structures of the vortex phases in regimes I–IV.

including the vortex lattice, the IMP (the ordered bubble and stripe phases), and the disordered or amorphous vortex phase.

In the high-field regime [IV in Fig. 1 and Fig. 2(a)], the vortices form the hexagonal Abrikosov lattice. As was mentioned earlier, the vortex lattice was initially predicted by the phenomenological GLAG theory for type-II/2 superconductors with $\kappa \gg 1$, $T \approx T_c$, and $H \approx H_{c2}$. In contrast, there are no restrictions on κ , T , and B that are needed to obtain this lattice in our simulation. It is well known that experiments indeed confirm the existence of the vortex lattice for type-II/2 superconductors at $T < T_c$ and $B < B_{c2}$. This result shows that our model is suitable for studying the vortex states for type-II/2 superconductors.^{28,29}

In the intermediate-field regime, that is, regimes II and III in Fig. 1, the vortex system displays two interesting superlattice patterns: (i) a hexagonal lattice of bubbles of vortices and (ii) parallel stripes of vortex collections. The details of the superlattices are shown in Figs. 2(c) and 2(b). As equilibrium vortex phases, these structures are, of course, the result of competition between the long-range repulsive interaction and the short-range attractive interaction at different vortex densities. These numerical superlattices coincide well with the experimental observation; see, for example, Fig. 4(c) in

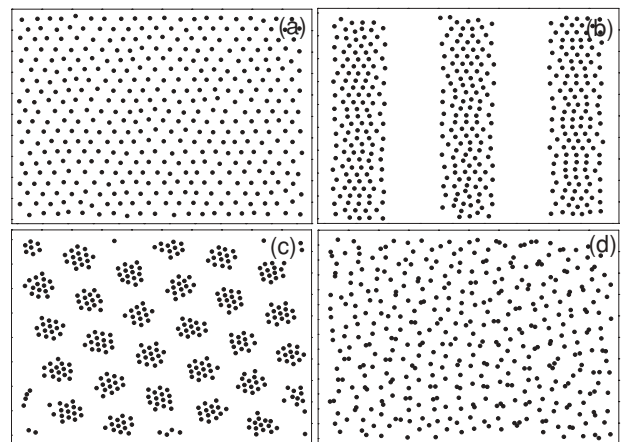


FIG. 2. Vortex phases for different magnetic fields at fixed temperature $T = 0$ and $N_v = 400$. Panel (a) shows the vortex lattice for $B = 0.8B_{c20}$. Panels (b) and (c) show the superlattice of vortex stripes for $B = 0.59B_{c20}$ and the superlattice of vortex bubbles for $B = 0.43B_{c20}$, respectively. Panel (d) shows the disordered phase for $B = 0.04B_{c20}$.

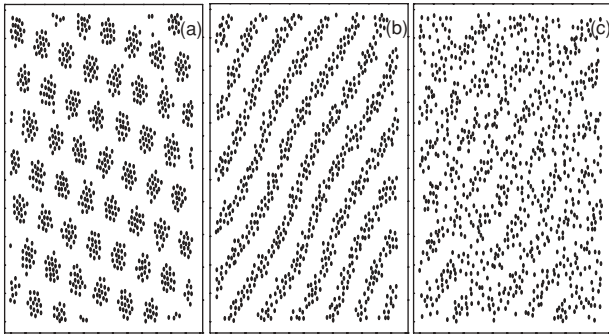


FIG. 3. Structures of the IMP as a function of temperature at $B = 0.43B_{c20}$: (a) superlattice of vortex bubbles at $T = 0.5T_c$; (b) vortex stripe phase at $T = 0.6T_c$; (c) liquid phase at $T = 0.75T_c$.

Ref. 11. To the best of our knowledge, this is the first report of reproducing the IMP through simulation. The intermediate-mixed state has been explained by the appearance of a long-range vortex attraction that causes an S-shape (unstable) magnetization curve from which the equilibrium states are obtained by a Maxwell construction.^{30,31} Note that we claim a long-range repulsion potential that is important for the formation of long-range order between vortex domains, such as stripes or bubbles [see Fig. 4(c) in Ref. 11]. This result shows that our model is also suitable for studying the vortex states for type-II/I superconductors.

In regime I in Fig. 1, the vortex system displays a disordered phase. The details of the corresponding patterns are shown in Figs. 2(d) and 3(c). At high temperatures for both low and high field, thermal fluctuation is important, so the vortices form a vortex liquid. We call it the high- T liquid. This high- T liquid state has been observed for both high- and low-temperature superconductors using various experimental techniques.³² While in the low-field regime for low temperature, the vortices are dilute and the disorders become important, and thus the vortex system manifests itself as an amorphous state.³³ This result is consistent with the prediction from the elastic theory.^{5,6} We also calculated the low-field vortex phase for the system without quenched disorders, and found that the vortex system will form an ordered vortex lattice after waiting for a very long relaxation time. This indicates that the formation

of a low-field disordered phase indeed results from the effect of quenched disorders. The existence of the disordered phases at both low temperatures (corresponding to low field) and high temperatures is reminiscent of the interesting reentrance melting phenomenon in vortex matter. It is clear that in the low- B regime of Fig. 1, the vortex phase experiences a transition from the IMP into the low- B disordered phase with decreasing field. In the high- B or intermediate- B regime, the vortex phase has a transition from the vortex lattice or the IMP into the high- T liquid upon increasing field or temperature; see also Fig. 3. In fact, the reentrance of vortex melting has been predicted by theory and confirmed by experiments.⁵⁻⁹

We then study the vortex phases as functions of field B and κ (and/or q). In Fig. 4(a), the B - κ phase diagram shows four typical vortex phases: a disordered vortex phase forms in lower fields, while in high fields, with increasing κ , vortices form a hexagonally ordered bubble phase and an ordered stripe phase, as well as a vortex lattice. The structures of these phases can be seen in Fig. 2. To understand the reason for the formation of these vortex phases as a function of κ , we show the representative intervortex interaction force $F^{vv}(r)$ curves for different κ , as shown in the inset of Fig. 4(a). For a larger κ , it is seen that $F^{vv}(r)$ is positive, meaning the intervortex interaction is pure repulsion. So vortices form an ordered lattice. For a smaller κ , $F^{vv}(r)$ becomes negative in a shorter range while still positive in a longer range. That is, this sort of interaction between particles (vortices) is of long-range repulsive with short-range attractive type. It has been well known that such types of interaction can lead to spatially periodic modulated structures in various condensed systems.¹⁵ For the superconducting vortex system studied here, the formation of vortex clusters such as bubblelike or stripelike structures is induced by short-range attraction. Additionally, the creation of intercluster order and intracluster order results from long-range repulsion and short-range repulsion respectively. On the other hand, the average distance between vortices in the initial stage is mainly controlled by vortex density B . For lower B corresponding to larger vortex-vortex separation, the intervortex interaction is so weak that vortices can only form a disordered or amorphous phase. For higher B , the short-range repulsion may be dominant, leading to an ordered lattice phase.

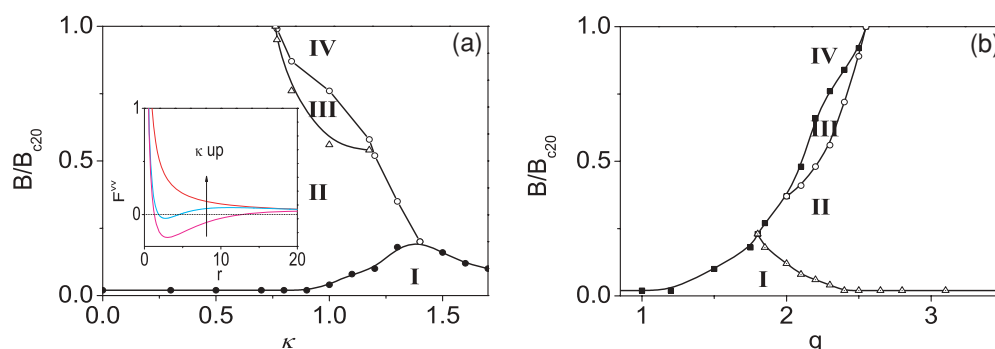


FIG. 4. (Color) (a) Phase diagram of vortex matter as function of field B and κ , (b) phase diagram of vortex matter as function of B and q for $T = 0$, $N_p = 2N_v$, $f_{pv} = 0.15f_0$, and $r_p = 0.2\lambda$. The phases in both (a) and (b) are the disordered vortex phase (I), the hexagonally ordered bubble phase (II), the ordered stripe phase (III), and the vortex lattice (IV). The inset in (a) shows the intervortex interaction force $F^{vv}(r)$ as a function of the distance r between vortices for different κ (see text for a more detailed discussion).

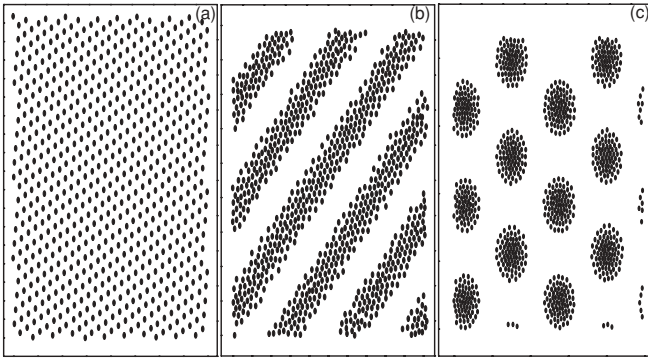


FIG. 5. Vortex phases for different q for $B = 0.65B_{c20}$, $T = 0$, $N_p = 2N_v$, $f_{pv} = 0.15f_0$, and $r_p = 0.2\lambda$: (a) the vortex lattice for $q = 0$; (b) the vortex stripe phase for $q = 2.3$; (c) the vortex bubble phase for $q = 3$.

The nature of the vortex system can also be examined by tuning the relative strength of the attraction to repulsion interactions q . Figure 5 shows three typical vortex phases for different q at a fixed field ($B = 0.65B_{c20}$). For $q = 0$, the

vortex system displays an ordered hexagonal lattice due to the dominant long-range repulsion [Fig. 5(a)]. With increasing q , the intervortex attraction becomes important. The long-range repulsion competes with the short-range attraction, resulting in the occurrence of a new characteristic length scale (the modulation period) relating to two kinds of spatially modulated structures: the vortex stripe phase and the bubble phase: for relatively small q (≈ 2.3), the vortex system exhibits two-dimensional symmetry [Fig. 5(b)], and for relatively large q (≈ 3), the vortex system shows three-dimensional symmetry [Fig. 5(c)]. In fact, the symmetry of two modulated structures is determined not only by q but also the vortex density B , because B controls the average vortex-vortex separation and thus the interaction between vortices. In Fig. 4(b), we show the vortex phase diagram as a function of B and q , displaying four typical vortex phases mentioned earlier. In addition to disordered phase in low fields, vortices form the vortex lattice, the ordered stripe phase, and the hexagonally ordered bubble phase depending on B and q .

One marked advantage of the molecular-dynamics simulation is that the time evolution of the formation of the previously mentioned phases can be studied. For simplicity,

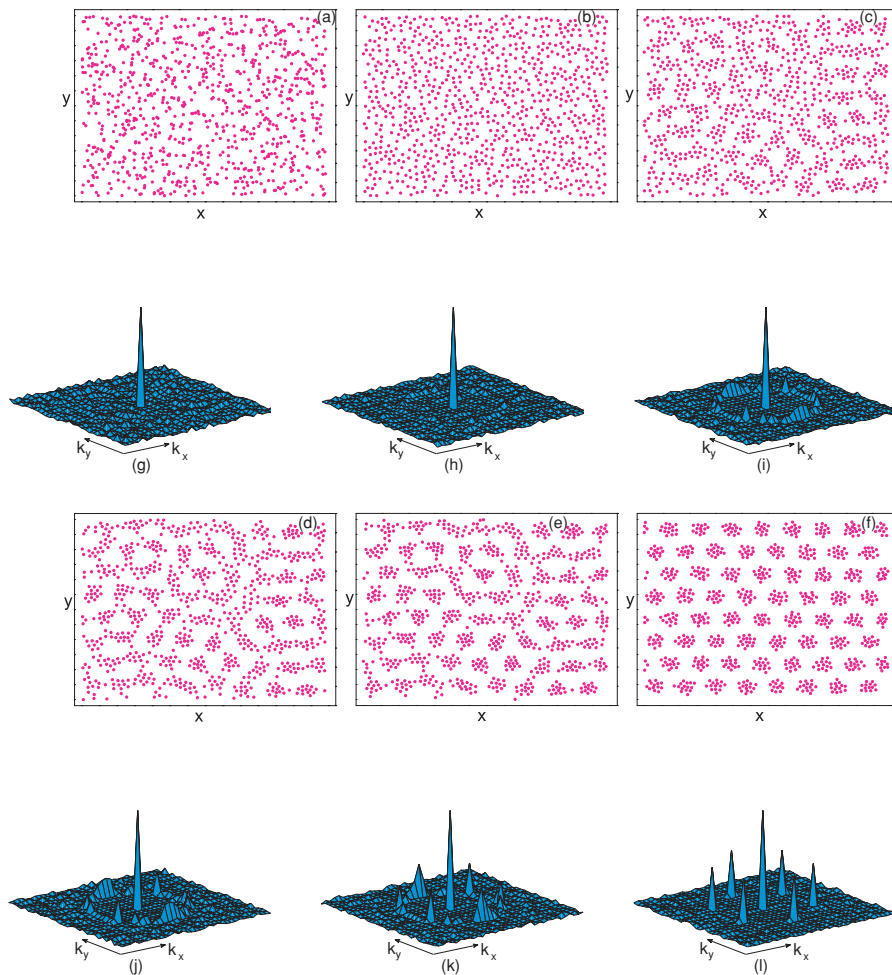


FIG. 6. (Color) Time evolution of the formation of the ordered bubble phase, starting from a random disordered state, as shown in (a), and the corresponding structure factors with $B = 0.43B_{c20}$ and $T = 0$. The vortex configurations are (b) $t = 2$, (c) $t = 10$, (d) $t = 20$, (e) $t = 30$, and (f) $t = 50$. The corresponding structure factor $S(k)$ are (g) $t = 0$, (h) $t = 2$, (i) $t = 10$, (j) $t = 20$, (k) $t = 30$, and (l) $t = 50$.

here we only show the formation of the superlattice of bubbles. The snapshots illustrated in Fig. 6 are the typical vortex structures with the corresponding structure factors, $S(\mathbf{k}) = |\sum_{i=1}^{N_v} \exp[i\mathbf{k} \cdot \mathbf{r}_i]|^2 / N_v$, at different times. It can be seen that the time evolution is characterized by two stages: an early stage dominated by vortex attraction and a late stage dominated by long-range vortex repulsion. In the early stage, the vortex system forms interconnected and irregular polydisperse domains [Figs. 6(b) and 6(c)]. The corresponding structure factors $S(k)$ show one central peak, indicating the absence of ordering [Figs. 6(h) and 6(i)]. In the late stage, as the long-range repulsive interaction becomes dominant, the bubbles of the vortex state become simultaneously monodisperse and ordered [Figs. 6(d)–6(f)], and the corresponding structure factors gradually become crystalline-like [Figs. 6(j)–6(l)].

In a real experiment, only part of the vortex states [Fig. 6(a)–6(f)] can be probed;¹² see also Fig. 4(b) in Ref. 11. For a perfect sample, the vortex relaxation time might be very short due to small local energy barriers. Thus, only the final equilibrium state [Fig. 6(f)] rather than the metastable states [Figs. 6(a)–6(e)] might be observed. However, for a sample with strong vortex pinning, the vortices are easily trapped, staying in the long-lived metastable states due to long relaxation time. This means that one can only record part of the metastable states rather than the equilibrium state [Fig. 6(f)]. This might explain why the disordered states have

been frequently observed for low- κ type-II superconductors¹² while the hexagonally ordered bubbles shown in Fig. 6(f) were seldom probed in experiments. For the sake of simplicity, we leave the effect of pinning centers on IMP and the corresponding vortex dynamics to a future study.

In summary, we have studied the phase diagram of type-II superconductors in the B - T , the B - κ , and B - q planes based on a molecular-dynamical simulation. The model we propose [Eq. (1)] to describe the complexity of the vortex state in superconductors provides short-range attraction and long-range repulsion and is a representative model for a class of physical systems with these properties. We have observed the IMP, the vortex lattice, and disordered phases over a wide range of fields and temperatures and κ . The IMP, consisting of a hexagonal superlattice of vortex bubbles or a superlattice of parallel stripes, has been numerically observed. The simulation results coincide well with the experimental observations for type-II superconductors with different κ .

X.B.X. is grateful to Professor E. H. Brandt for helpful discussions. This work was supported by grants from the Ministry of Science and Technology (MOST) 973 Program of China (No. 2011CBA00107, No. 2011CB933400, and No. 2008CB601003), the National Science Foundation (NSF) of China (No. 91021003 and No. 10674060), and the Jiangsu Province Foundation of Natural Science (No. BK2006109).

*xxb@nju.edu.cn

¹L. W. Shubnikov, W. I. Chotewitsch, J. D. Schepelew, and J. N. Rjabinin, *Zh. Eksp. Teor. Fiz.* **7**, 221 (1937).

²L. P. Gor'kov, *Zh. Eksp. Teor. Fiz.* **37**, 833 (1959) [*Sov. Phys. JETP* **10**, 593 (1960)].

³For a review see, e.g., P. G. de Gennes, *Superconductivity of Metal and Alloy* (Benjamin, New York, 1966).

⁴E. H. Brandt, *Phys. Rev. Lett.* **78**, 2208 (1997).

⁵G. Blatter, M. V. Feigel'man, V. B. Geshkenbein, A. I. Larkin, and V. M. Vinokur, *Rev. Mod. Phys.* **66**, 1125 (1994).

⁶T. Giamarchi and S. Bhattacharya, e-print [arXiv:cond-mat/0111052](https://arxiv.org/abs/cond-mat/0111052).

⁷S. S. Banerjee *et al.*, *Europhys. Lett.* **44**, 91 (1998).

⁸K. Ghosh *et al.*, *Phys. Rev. Lett.* **76**, 4600 (1996).

⁹C. J. Olson, C. Reichhardt, R. T. Scalettar, G. T. Zimányi, and N. Grønbech-Jensen, *Physica C* **384**, 143 (2003).

¹⁰H. Träuble *et al.*, *Phys. Status Solidi* **20**, 95 (1967); U. Essmann, *Phys. Lett. A* **41**, 477 (1972); B. Obst, *Phys. Status Solidi B* **45**, 467 (1971); J. Auer and H. Ullmaier, *Phys. Rev. B* **7**, 136 (1973).

¹¹E. H. Brandt, *Rep. Prog. Phys.* **58**, 1465 (1995).

¹²R. P. Huebener, *Magnetic Flux Structures in Superconductors* (Springer-Verlag, New York, 1979).

¹³A. Glatz, I. Aranson, V. Vinokur, N. Chitchev, and T. Baturina, e-print [arXiv:0910.0659](https://arxiv.org/abs/0910.0659) [cond-mat].

¹⁴L. Kramer, *Phys. Rev. B* **3**, 3821 (1971).

¹⁵M. Seul and D. Andelman, *Science* **267**, 476 (1995).

¹⁶F. Sciortino, S. Mossa, E. Zaccarelli, and P. Tartaglia, *Phys. Rev. Lett.* **93**, 055701 (2004).

¹⁷A. Stradner, H. Sedgwick, F. Cardinaux, W. C. K. Poon, S. U. Egelhaaf, and P. Schurtenberger, *Nature (London)* **432**, 492 (2004).

¹⁸F. Sciortino, P. Tartaglia, and E. Zaccarelli, *J. Phys. Chem. B* **109**, 21942 (2005).

¹⁹J. Chakrabarti, S. Chakrabarti, and H. Löwen, *J. Phys. Condens. Matter* **18**, L81 (2006).

²⁰R. P. Sear, S. W. Chung, G. Markovich, W. M. Gelbart, and J. R. Heath, *Phys. Rev. E* **59**, R6255 (1999).

²¹B. P. Stojković, Z. G. Yu, A. R. Bishop, A. H. Castro Neto, and N. Grønbech-Jensen, *Phys. Rev. Lett.* **82**, 4679 (1999).

²²C. Reichhardt, C. J. Olson Reichhardt, I. Martin, and A. R. Bishop, *Phys. Rev. Lett.* **90**, 026401 (2003).

²³A. B. Kolton, D. Domínguez, and N. Grønbech-Jensen, *Phys. Rev. Lett.* **83**, 3061 (1999).

²⁴X. B. Xu, H. Fangohr, X. N. Xu, M. Gu, Z. H. Wang, S. M. Ji, S. Y. Ding, D. Q. Shi, and S. X. Dou, *Phys. Rev. Lett.* **101**, 147002 (2008).

²⁵H. Fangohr, A. Price, S. Cox, P. A. J. de Groot, G. J. Daniell, and K. S. Thomas, *J. Comput. Phys.* **162**, 372 (2000).

²⁶H. J. Jensen, A. Brass, A. C. Shi, and A. J. Berlinsky, *Phys. Rev. B* **41**, 6394 (1990).

²⁷M. Tinkham, *Introduction to Superconductivity* (McGraw Hill, New York, 1975).

²⁸H. Fangohr, S. J. Cox, and P. A. J. de Groot, *Phys. Rev. B* **64**, 064505 (2001).

²⁹C. Reichhardt and C. J. Olson Reichhardt, *Phys. Rev. B* **66**, 172504 (2002).

³⁰E. H. Brandt and S. P. Zhou, *Physics* **2**, 22 (2009).

³¹V. Moshchalkov, M. Menghini, T. Nishio, Q. H. Chen, A. V. Silhanek, V. H. Dao, L. F. Chibotaru, N. D. Zhigadlo, and J. Karpinski, *Phys. Rev. Lett.* **102**, 117001 (2009).

³²See, e.g., X. S. Ling, S. R. Park, B. A. McClain, S. M. Choi, D. C. Dender, and J. W. Lynn, *Phys. Rev. Lett.* **86**, 712 (2001).

³³D. R. Nelson, *Phys. Rev. Lett.* **60**, 1973 (1988).